
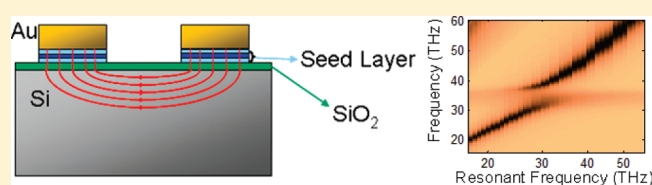


Strong Coupling between Nanoscale Metamaterials and Phonons

D.J. Shelton,^{*,†,⊥} I. Brener,^{‡,§} J. C. Ginn,^{‡,§,⊥} M. B. Sinclair,[‡] D. W. Peters,[‡] K. R. Coffey,^{||} and G. D. Boreman[†][†]CREOL, University of Central Florida, 4000 Central Florida Boulevard, Orlando, Florida 32816, United States[‡]Sandia National Laboratories, P.O. 5800, Albuquerque New Mexico 87185-1082, United States[§]Center for Integrated Nanotechnologies, P.O. Box 5800, Albuquerque, New Mexico 87185, United States^{||}AMPAC, University of Central Florida, 4000 Central Florida Boulevard, Orlando, Florida 32816, United States[⊥]Plasmonics Inc., 12565 Research Parkway, STE 300, Orlando, Florida 32826, United States Supporting Information

ABSTRACT: We use split ring resonators (SRRs) at optical frequencies to study strong coupling between planar metamaterials and phonon vibrations in nanometer-scale dielectric layers. A series of SRR metamaterials were fabricated on a semiconductor wafer with a thin intervening SiO₂ dielectric layer. The dimensions of the SRRs were varied to tune the fundamental metamaterial resonance across the infrared (IR) active phonon band of SiO₂ at 130 meV (31 THz). Strong anticrossing of these resonances was observed, indicative of strong coupling between metamaterial and phonon excitations. This coupling is very general and can occur with any electrically polarizable resonance including phonon vibrations in other thin film materials and semiconductor band-to-band transitions in the near to far IR. These effects may be exploited to reduce loss and to create unique spectral features that are not possible with metamaterials alone.

KEYWORDS: Metamaterials, phonon vibrational modes, normal mode splitting, split ring resonators, near fields



A metamaterial is a composite comprising subwavelength spaced inclusions embedded in a dielectric matrix and exhibiting effective electromagnetic properties. Metamaterials give rise to new capabilities for the manipulation of electromagnetic radiation, such as left handed refraction, nondiffraction limited imaging and cloaking (for a review, see refs 1 and 2). At optical frequencies (visible or infrared), these artificial materials require nanofabrication since the dimensions of the individual elements are a small fraction of the wavelength of operation. Examples of metamaterial elements used at optical frequencies include layered dipoles,³ three-dimensional (3D) fishnets,⁴ splitting resonators (SRR),⁵ and more advanced capacitive gap designs.⁶

The issue of interactions between different types of engineered resonances has received considerable attention since it was shown that electromagnetically induced transparency behavior can be mimicked using coupling between metamaterials and/or plasmonic resonators.^{7–10} Aside from the interesting fundamental phenomena that arise in these coupled systems, this approach could lead to lower-loss metamaterial designs.¹⁰ Much of the published work has explored interactions between nanoresonators of similar nature (i.e., coupled metamaterial or plasmonic structures) either with different geometrical coupling parameters¹⁰ or using higher-order multipole modes.¹¹ It has also been reported that surfaces structured with nanoscale features can mimic surface plasmon polariton behavior and dispersion relationships.^{12,13} The coupling of these plasmons to other fundamental excitations with dipole-like transitions can lead to mixed plasmon-polariton modes. For example, this has

been observed in exciton-plasmon coupled systems¹⁴ and phonon-plasmon modes.^{15,16} Also, the interaction between infrared plasmons and phonons has been used for sensing applications using surface-enhanced infrared absorption (SEIRA).^{17–20}

In this paper we explore the coupling between metamaterial resonators and infrared active phonons. We show that these two resonators can couple strongly, leading to normal mode splitting similar to vacuum-Rabi splitting that occurs with optical emitters coupled to microcavities²¹ or plasmonic resonances.^{22–24} The observed anticrossing behavior results in the opening of a transparency window within the absorption band of the uncoupled metamaterial. The amount of coupling can be altered through the design of the metamaterial resonators, the proximity of the dielectric film containing the vibrational species to the resonator, the dielectric film thickness, and the amount of field overlap with the dielectric layer. This new approach could have important implications for the design of future active and nonlinear metamaterials, and plasmonic filters.

The metamaterial resonator we chose to use is the split-ring resonator.⁵ The lowest resonant mode of the SRR is an inductive resonance that can lead to negative permeability when excited in a TM geometry. The lowest mode can also be excited at normal incidence (TE geometry) due to bianisotropy and degeneracy.²⁵ The frequency of the fundamental resonance scales linearly from radio frequencies to the near-infrared,²⁶ however, the *Q* of this resonance degrades as the frequency approaches the visible part

Received: March 1, 2011

Published: April 04, 2011

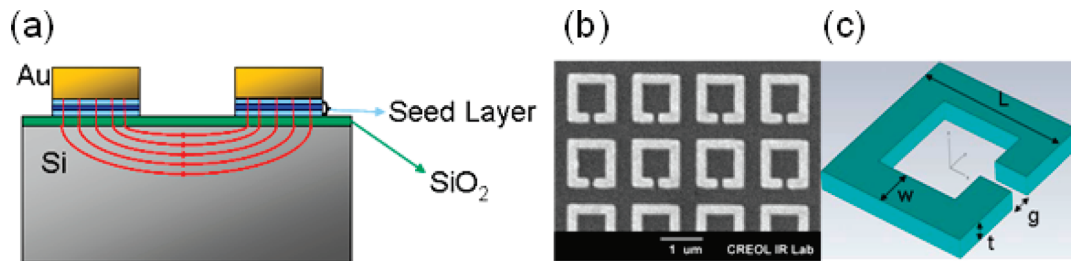


Figure 1. (a) Schematic cross section showing thin film interface between metallic SRR elements and Si wafer including a thin SiO₂ layer. (b) An SEM micrograph of the SRR arrays. (c) Definition of dimensional parameters as shown in Table 1.

of the spectrum due to ohmic losses in the metals. We can characterize the lowest resonance of the SRR through two parameters, its resonant frequency (ω_{MM}) and its damping rate (γ_{MM}) defined as the full-width at half-maximum of the spectral transmission minimum centered at ω_{MM} . The resonant frequency of a nominally lossless metamaterial can be found using an LC circuit-equivalent such that ω_{MM} is defined by

$$\omega_{\text{MM}} = \sqrt{\frac{1}{LC}} = \sqrt{\frac{1}{L(C_g + C_f)}} \quad (1)$$

where the inductance (L) and capacitance (C) may be computed for an SRR based upon the dimensions of the element as described in ref 27. The element capacitance for an SRR element is the summation of the gap capacitance (C_g) and fringing-field capacitance (C_f). The C_f contribution to ω_{MM} is strongly affected by the presence of low-refractive-index layers such as native oxides or adhesion layers between the SRR elements and high refractive index substrates such as Si or GaAs.^{27,28}

The damping rate γ_{MM} depends upon the ohmic loss and the geometry of the metamaterial elements and may be determined from numerical-electromagnetic simulation using measured optical constants as is done in this article, or it may be determined analytically using a circuit-equivalent model.²⁹ Using ω_{MM} and γ_{MM} , the extinction spectrum, $\alpha(\omega)$, of the uncoupled metamaterial resonator can be analytically described by a Lorentzian line shape

$$\alpha_{\text{MM}}(\omega) = \frac{A\gamma_{\text{MM}}}{(\omega - \omega_{\text{MM}})^2 + \gamma_{\text{MM}}^2} \quad (2)$$

where A is a parameter that describes the strength of the absorption. We may write a similar expression for the uncoupled IR active phonon mode of an isotropic dielectric layer, given its resonant frequency (ω_{ph}) and damping rate (γ_{ph}).

Figure 1 shows one possible cross section configuration in which a dielectric film is in contact with metamaterial elements. Assuming only one phonon mode is present in the film, this system can be represented as two coupled damped harmonic oscillators. When significant coupling occurs, normal mode splitting will result in two new Lorentzian-like resonances with distinct eigenfrequencies and damping rates. The coupled mode equations may then be solved³⁰ to obtain

$$V^2 = (\omega_{\text{MM}} - \omega - i\gamma_{\text{MM}}\omega)(\omega_{\text{ph}} - \omega - i\gamma_{\text{ph}}\omega) \quad (3)$$

where V^2 describes the coupling strength that is due to the spatial overlap of the SRR near-field and the dielectric film. The real parts of the two solutions of eq 3 are the eigenfrequencies of the metamaterial-phonon coupled system, while the imaginary parts

of the solutions are the damping rates of the normal modes. When multiple phonon modes are present near ω_{MM} , a series of second order linear differential equations may be formed by summing over all the modes present.

The coupling strength determines how close ω_{MM} and ω_{ph} need to be for normal mode splitting to occur. Mode splitting results in the formation of a forbidden energy gap, Ω , that may be measured experimentally as a transparency window. This behavior is analogous to quantum level repulsion or anticrossing. The energy gap Ω may be related to the coupling constant V ³⁰

$$\Omega = \sqrt{4V^2 - (\gamma_{\text{MM}} - \gamma_{\text{ph}})^2} \quad (4)$$

Strong coupling will not occur when ω_{MM} and ω_{ph} are spectrally spaced by energy greater than Ω . Thus, a matrix formulation for multiple phonon modes should only be needed in cases where modes lie within Ω of each other.

To demonstrate the expected anticrossing behavior, seven SRR metamaterial-element planar-arrays with different element dimensions were fabricated on a 10 nm thick SiO₂ film. Changing the dimensions of the element allowed the metamaterial resonance frequency ω_{MM} to be scanned across the dielectric phonon mode. SiO₂ was selected for the thin film because it is easy to deposit with accurate thickness, and the Si–O phonon absorption band near 9 μm is ideal for coupling experiments in the thermal IR. The 10 nm film thickness was chosen so that a significant fraction of the near fields of the elements would be confined in the thin-film, ensuring strong coupling.²⁷ Furthermore, keeping the film thickness small minimizes the direct absorption of the incident radiation by the TO phonon mode that would be detected during measurements regardless of the presence of a metamaterial layer.

An SEM image of the fabricated SRR elements is shown in Figure 1b along with a schematic diagram showing the SRR dimensions (Figure 1a,c). The SRR elements were fabricated using electron-beam lithography and a lift-off process. The elements were metalized with 75 nm of Au with a 5 nm Ti adhesion layer deposited by electron-beam evaporation. The SiO₂ was deposited onto a Si wafer using electron-beam evaporation monitored by in situ ellipsometry using a J.A. Woollam M-2000 system. The measured SiO₂ thickness includes the thickness of the native oxide of the Si wafer. After deposition, we used IR ellipsometry in order to directly measure the dielectric function $\epsilon(\omega)$ of the evaporated SiO₂. The phonon resonant frequency was measured to be $\omega_{\text{ph}} = 130$ meV (31 THz) and its damping rate is $\gamma_{\text{ph}} = 11.3$ meV.

Table 1 shows the calculated values for the resonant frequency and the uncoupled damping rate of the SRRs in the absence of the vibrational mode in the oxide layer. These calculations were

Table 1. Dimensions of the SRR Elements Used in the Experiment along with the Calculated Resonant Frequencies and Damping Rates

L , nm	g , nm	w , nm	period, nm	ω_{MM} , meV	γ_{MM} , meV
520	80	100	720	186	96.7
590	100	120	830	165	85.8
660	110	140	930	148	71.9
690	110	140	970	141	69.7
740	120	150	1000	133	66.4
880	140	180	1230	112	59.1
1100	160	200	1530	90	46.9

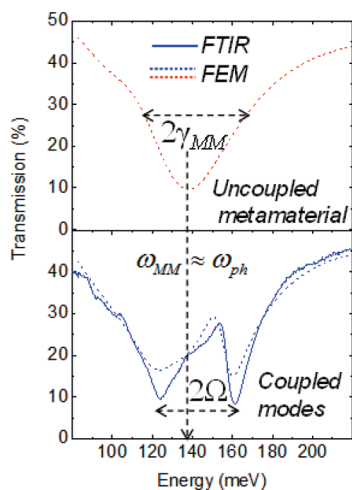


Figure 2. The simulated spectral transmission of the SRR metamaterial without the influence of phonons in the 10 nm thick SiO₂ film (top) compared to the measured and simulated normal mode splitting that occurs for an SRR metamaterial when the phonon modes are present in SiO₂ film (bottom).

performed using finite-element method (FEM) simulation (Ansoft HFSS) and by assuming a dispersionless SiO₂ film with refractive index equal to 1.45. The dispersionless SiO₂ was included to account for the fringing-field capacitance contribution to the resonant frequency as described by eq 1. The FEM simulation also included the effects of the seed layer and the measured optical constants of the metals.

The upper panel of Figure 2 shows an FEM simulation of the transmission spectrum of an SRR array on a dispersionless SiO₂ layer. For this array, the uncoupled resonant frequency ω_{MM} is nearly equal to the phonon resonant frequency ω_{ph} and the SRR damping rate γ_{MM} was found to be 25 meV. The bottom panel of Figure 2 shows the agreement between the measured transmission spectrum and FEM simulation for the real SiO₂ film including the phonon modes. The two resonant modes repel each other resulting in new coupled modes that produce a unique dual resonance in the transmission spectrum. By equating the spectral location of the two transmission minima to the eigenfrequencies of the coupled system, the energy gap (Ω) for this system was found to be 37 meV. According to eq 4 this results in a coupling constant V equal to 17 meV.

Figure 3a shows the measured transmission spectra for the seven SRR element arrays. As the bare metamaterial resonant frequency is scanned across the IR band from 5 to 15 μm

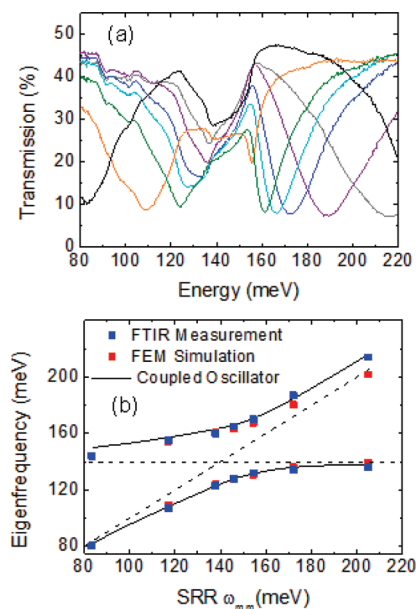


Figure 3. (a) The measured transmission spectra of the seven SRR metamaterial arrays in contact with an SiO₂ film (dimensions shown in Table 1). (b) The measured resonant frequencies of the coupled modes compared to the analytical model for two coupled oscillators.

(~ 80 – 200 meV), anticrossing behavior is observed between the two eigenfrequencies. An energy gap forms around ω_{ph} where neither the metamaterial nor the phonon modes absorb. Shown in Figure 3b is the dispersion of the coupled metamaterial-phonon system. These curves were obtained by plotting the measured eigenfrequencies along with the numerically simulated eigenfrequencies of the coupled system versus the uncoupled metamaterial resonant frequencies found in Table 1. The analytical model is shown as the solid curve that was calculated using the measured value for V , ω_{ph} , γ_{ph} and the values for ω_{MM} and γ_{MM} from Table 1. The broken lines in Figure 3b show the light line (eigenfrequency equal to the uncoupled SRR mode energy) and the resonant energy of the phonon mode. Away from the energy gap where ω_{MM} is equal to ω_{ph} , the data should converge to these values. The dispersion curves in Figure 3b demonstrate agreement between the measurements, the numerical simulations, and the analytical model.

Finally, we show how the coupling strength can be controlled by fabrication parameters such as the location of the dielectric layer with respect to the metamaterials resonators. As shown in the schematic diagram of Figure 1a, a strong interaction between the metamaterial and the phonon resonance can be expected as long as the dielectric layer has significant overlap with the electric field lines at resonance. FEM and FDTD simulations confirm that the field lines decay quickly into the substrate and that the depth for effective interaction is of the order of the gap distance. Using FDTD simulations (see Supporting Information) we studied the variation of metamaterial-phonon coupling strength with respect to the location of a fixed 10 nm layer of SiO₂ underneath the metallic traces, while keeping all the other parameters unchanged. Figure 4a shows the anticrossing curve obtained when the SiO₂ is directly in contact with the SRRs, while for Figure 4b the SiO₂ layer was placed 50 nm below the SRRs and for Figure 4c the SiO₂ layer was placed 125 nm below the metal traces. By fitting the anticrossing curves obtained from

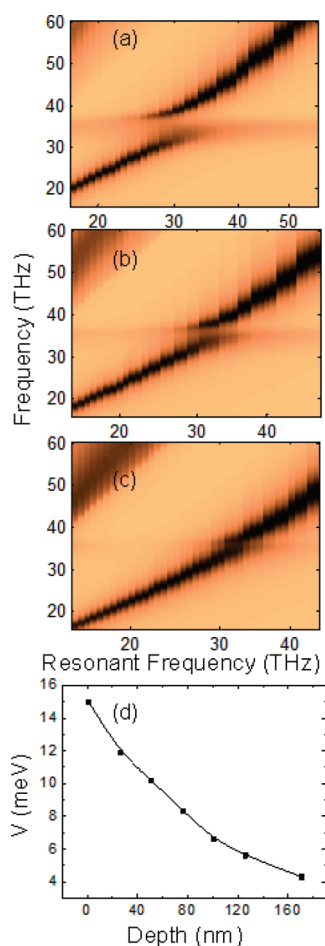


Figure 4. Normal mode splitting simulated by FDTD as the SiO₂ layer is displaced from the SRR metamaterial elements: (a) SiO₂ in contact, (b) SiO₂ depth of 50 nm, (c) SiO₂ depth = 125 nm. (d) The coupling coefficient V derived from the FDTD simulations is plotted as a function of the depth of the SiO₂ layer.

the FDTD simulations to eq 3, it is possible to plot the variation of the coupling strength as a function of the depth parameter. Figure 4d shows the manner in which the coupling strength diminishes with depth. Clearly, the coupling vanishes for depths greater than ~ 200 nm, which roughly corresponds to the penetration depth of the fringing fields caused by the metamaterial resonators. This is a powerful way to tune the coupling strength between metamaterials and phonon modes in a neighboring dielectric layer and can be used as an additional degree of freedom for the design of eigenmode spectral features with frequency, spacing, and bandwidth that may not be achievable with a single layer of metamaterial elements. When the metamaterial is strongly coupled to these phonons (i.e., the dielectric layer is close to the metal lines), the numerical simulations show that the magnitude of the electromagnetic fields is the strongest inside the dielectric layer (Supporting Information). This is in contrast to the conventional wisdom on field enhancement using various types of nanoplasmonic resonators or small metallic gaps where the maximum field strength is reached close to the surface or near the metallic edges.

In summary, we have demonstrated that strong coupling can occur between the resonances of planar metamaterial elements and phonon-vibrational modes. Specifically, we have shown

experimentally that the characteristic anticrossing dispersion relationship of coupled metamaterial-phonon modes is obtained for metamaterial systems comprising a single layer of SRR elements in contact with a 10 nm thick SiO₂ film. These experimental results are in agreement with full-wave electromagnetic simulations, as well as a phenomenological model. The physical nature of these strong coupling phenomena was further investigated by showing that the coupling strength decreases monotonically as the nanometer-scale SiO₂ layer is displaced from the metamaterial elements. These results indicate that strong coupling arises due to the interaction between the near fields at the metal-dielectric interface and the vibrational modes in the dielectric layer. Since this near field behavior exists for any metamaterial element type, we conclude that strong coupling between metamaterial elements and phonon modes is a general phenomenon.

■ ASSOCIATED CONTENT

S Supporting Information. Supporting Information includes details of the FEM and FDTD calculations as well as measured optical properties of the materials used in these experiments including Au and SiO₂. This material is available free of charge via the Internet at <http://pubs.acs.org>.

■ AUTHOR INFORMATION

Corresponding Author

*E-mail: david.shelton@plasmonics-inc.com.

■ ACKNOWLEDGMENT

This research was supported by the Laboratory Directed Research and Development program at Sandia National Laboratories. Sandia is a multiprogram laboratory operated by Sandia Corporation, a Lockheed Martin Company, for the United States Department of Energy's National Nuclear Security Administration under Contract DE-AC04-94AL85000. This work was performed, in part, at the Center for Integrated Nanotechnologies, a U.S. Department of Energy, Office of Basic Energy Sciences user facility. The simulation portion was funded by the Energy Frontier Research Center for Solid State Lighting Science. We also acknowledge funding by DARPA/MTO's Casimir Effect Enhancement program under DOE/NNSA Contract DE-AC52-06NA25396.

■ REFERENCES

- (1) Cai, W.; Shalae, V. *Optical Metamaterials: Fundamentals and Applications*; Springer: New York, 2009.
- (2) Cui, T.; Smith, D.; Liu, R. *Metamaterials: Theory, Design, and Applications*; Springer: New York, 2009.
- (3) Podolskiy, V.; Sarychev, A.; Shalae, V. Plasmon modes and negative refraction in metal nanowire composites. *Opt. Express* **2003**, *11* (7), 735–745.
- (4) Zhang, S.; Fan, W.; Panoiu, N.; Malloy, K.; Osgood, R.; Brueck, S. Experimental demonstration of near-infrared negative-index metamaterials. *Phys. Rev. Lett.* **2005**, *95* (13), 137404.
- (5) O'Brien, S.; Pendry, J. Magnetic activity at infrared frequencies in structured metallic photonic crystals. *J. Phys.: Condens. Matter* **2002**, *14*, 6383.
- (6) Chen, H.; O'Hara, J.; Azad, A.; Taylor, A.; Averitt, R.; Shrekenhamer, D.; Padilla, W. Experimental demonstration of frequency-agile terahertz metamaterials. *Nat. Photonics* **2008**, *2* (5), 295–298.

- (7) Liu, N.; Langguth, L.; Weiss, T.; Kastel, J.; Fleischhauer, M.; Pfau, T.; Giessen, H. Plasmonic analogue of electromagnetically induced transparency at the Drude damping limit. *Nat. Mater.* **2009**, *8* (9), 758–762.
- (8) Liu, N.; Weiss, T.; Mesch, M.; Langguth, L.; Eigenthaler, U.; Hirscher, M.; Sonnichsen, C.; Giessen, H. Planar Metamaterial Analogue of Electromagnetically Induced Transparency for Plasmonic Sensing. *Nano Lett* **2010**, *10* (4), 1103–1107.
- (9) Papasimakis, N.; Fedotov, V.; Zheludev, N.; Prosvirnin, S. Metamaterial Analog of Electromagnetically Induced Transparency. *Phys. Rev. Lett.* **2008**, *101* (25), 253903.
- (10) Tassin, P.; Zhang, L.; Koschny, T.; Economou, E.; Soukoulis, C. Low-Loss Metamaterials Based on Classical Electromagnetically Induced Transparency. *Phys. Rev. Lett.* **2009**, *102* (5), 053901.
- (11) Liu, N.; Langguth, L.; Weiss, T.; Kästel, J.; Fleischhauer, M.; Pfau, T.; Giessen, H. Plasmonic analogue of electromagnetically induced transparency at the Drude damping limit. *Nat. Mater.* **2009**, *8* (9), 758–762.
- (12) Maier, S.; Andrews, S.; Martin-Moreno, L.; Garcia-Vidal, F. Terahertz surface plasmon-polariton propagation and focusing on periodically corrugated metal wires. *Phys. Rev. Lett.* **2006**, *97* (17), 176805.
- (13) Pendry, J.; Martin-Moreno, L.; Garcia-Vidal, F. Mimicking surface plasmons with structured surfaces. *Science* **2004**, *305* (5685), 847.
- (14) Vasa, P.; Pomraenke, R.; Schwieger, S.; Mazur, Y.; Kunets, V.; Srinivasan, P.; Johnson, E.; Kihm, J.; Kim, D.; Runge, E. Coherent Exciton–Surface-Plasmon-Polariton Interaction in Hybrid Metal-Semiconductor Nanostructures. *Phys. Rev. Lett.* **2008**, *101* (11), 116801.
- (15) Neubrech, F.; Pucci, A.; Cornelius, T.; Karim, S.; García-Etxarri, A.; Aizpurua, J. Resonant Plasmonic and Vibrational Coupling in a Tailored Nanoantenna for Infrared Detection. *Phys. Rev. Lett.* **2008**, *101*, 15.
- (16) Neubrech, F.; Weber, D.; Enders, D.; Nagao, T.; Pucci, A. Antenna Sensing of Surface Phonon Polaritons. *J. Phys. Chem. C* **2010**, *114* (16), 7299–7301.
- (17) Hartstein, A.; Kirtley, J. R.; Tsang, J. C. Enhancement of the Infrared Absorption from Molecular Monolayers with Thin Metal Overlayers. *Phys. Rev. Lett.* **1980**, *45* (3), 201.
- (18) Jensen, T. R.; Duyne, R. P. V.; Johnson, S. A.; Maroni, V. A. Surface-Enhanced Infrared Spectroscopy: A Comparison of Metal Island Films with Discrete and Nondiscrete Surface Plasmons. *Appl. Spectrosc.* **2000**, *54*, 371–377.
- (19) Kundu, J.; Le, F.; Nordlander, P.; Halas, N. J. Surface enhanced infrared absorption (SEIRA) spectroscopy on nanoshell aggregate substrates. *Chem. Phys. Lett.* **2008**, *452* (1–3), 115–119.
- (20) Rodriguez, K. R.; Shah, S.; Williams, S. M.; Teeters-Kennedy, S.; Coe, J. V. Enhanced infrared absorption spectra of self-assembled alkanethiol monolayers using the extraordinary infrared transmission of metallic arrays of subwavelength apertures. *J. Chem. Phys.* **2004**, *121* (18), 8671–8675.
- (21) Thompson, R.; Rempe, G.; Kimble, H. Observation of normal-mode splitting for an atom in an optical cavity. *Phys. Rev. Lett.* **1992**, *68* (8), 1132–1135.
- (22) Dintinger, J.; Klein, S.; Bustos, F.; Barnes, W. L.; Ebbesen, T. W. Strong coupling between surface plasmon-polaritons and organic molecules in subwavelength hole arrays. *Phys. Rev. B* **2005**, *71* (3), 035424.
- (23) Gómez, D. E.; Vernon, K. C.; Mulvaney, P.; Davis, T. J. Surface Plasmon Mediated Strong Exciton-Photon Coupling in Semiconductor Nanocrystals. *Nano Lett.* **2009**, *10* (1), 274–278.
- (24) Passmore, B. S.; Adams, D. C.; Ribaudou, T.; Wasserman, D.; Lyon, S.; Davids, P.; Chow, W. W.; Shaner, E. A. Observation of Rabi Splitting from Surface Plasmon Coupled Conduction State Transitions in Electrically Excited InAs Quantum Dots. *Nano Lett.* **2011**, *11* (2), 338–342.
- (25) Smith, D.; Gollub, J.; Mock, J.; Padilla, W.; Schurig, D. Calculation and measurement of bianisotropy in a split ring resonator metamaterial. *J. Appl. Phys.* **2006**, *100*, 024507.
- (26) Zhou, J.; Koschny, T.; Kafesaki, M.; Economou, E.; Pendry, J.; Soukoulis, C. Saturation of the magnetic response of split-ring resonators at optical frequencies. *Phys. Rev. Lett.* **2005**, *95* (22), 223902.
- (27) Shelton, D. J.; Peters, D. W.; Sinclair, M. B.; Brener, I.; Warne, L. K.; Basilio, L. I.; Coffey, K. R.; Boreman, G. D. Effect of thin silicon dioxide layers on resonant frequency in infrared metamaterials. *Opt. Express* **2010**, *18* (2), 1085–1090.
- (28) O'Hara, J. F.; Singh, R.; Brener, I.; Smirnova, E.; Han, J.; Taylor, A. J.; Zhang, W. Thin-film sensing with planar terahertz metamaterials: sensitivity and limitations. *Opt. Express* **2008**, *16* (3), 1786–1795.
- (29) Ginn, J.; Shelton, D.; Krenz, P.; Lail, B.; Boreman, G. Altering infrared metamaterial performance through metal resonance damping. *J. Appl. Phys.* **2009**, *105*, 7.
- (30) Kavokin, A.; Baumberg, J.; Malpuech, G.; Laussy, F. *Microcavities*; Oxford University Press: New York, 2007.